10th Pacific Symposium on Flow Visualization and Image Processing
Naples, Italy, 15-18 June, 2015

Numerical visualization of nappe oscillation

Michele Girfoglio[1,*], Fortunato De Rosa[1], Gennaro Coppola[1], Luigi de Luca[1]

[1]Department of Industrial Engineering (DII), University of Naples Federico II, Naples, Italy
[*]corresponding author: michele.girfoglio@unina.it

Abstract The unsteady global dynamics of a gravitational liquid sheet interacting with a onesided adjacent air enclosure, typically referred to as nappe oscillation, is addressed, under the assumptions of potential flow and presence of surface tension effects. Preliminary physical insights of the sheet centerline sinuous modes show that the nappe dynamics features the propagation of two wave fronts both directed downstream or one downstream and the other one upstream depending on whether the flow Weber number is greater or less than unity, respectively; moreover, the overall system behaves as a driven damped spring-mass oscillator, where the liquid sheet acts as the mass and the air enclosure as the spring. The findings of the eigenvalues spectral analysis closely agree with direct numerical simulations of the partial differential equation governing in the space-time domain the global evolution of the disturbances, starting from an initial gaussian-like shape.
Keywords: liquid sheet, surface tension, numerical visualization

1 Introduction

It is well known that a thin water sheet (curtain), flowing freely from a top opening, gives rise to strong low-frequency periodic oscillations when interacting with an air enclosure acting as a resonator. Such a behavior, commonly referred to as the nappe oscillation phenomenon, has been theoretically addressed by Schmid and Henningson [1], who formulated the linearized physical model governing the spatio-temporal evolution of disturbances in the form of an integro-differential system of equations over a finite length domain. Within the framework of the linear non-modal stability theory, they found time-periodic oscillations of the amplification of the disturbance energy, and correlated the period of such oscillations to the quasi-constant spacing among the imaginary part of the eigenvalues. They concluded that the phenomenon under study is governed not by a single mode but by the (linear) interaction of many (stable) modes. Such a global feature of the spectrum closely agrees with the low-frequency oscillations typically observed during the nappe oscillation. Since the role played by viscosity and surface tension should be important in stabilizing the spectrum, as argued by the authors themselves, they limited the analysis to some significant stable modes, focusing their interest on the global oscillations; no connection with parameters associated with single modes was inspected. In the present work, the nappe oscillation problem is revisited from the linear global viewpoint, by taking into account the surface tension effects. The study is based on a simplified one-dimensional unsteady model, already derived in the different context of the modeling of slender liquid sheets by means of a series expansion in the slenderness parameter for the unknown flow quantities ([2], [3]). The model is closed with the specification of the external pressure field, representing the reaction of an air enclosure located on one side of the sheet. The problem is investigated theoretically, by employing both modal analysis, and numerically, by means of direct numerical simulation of the unsteady equations.

2 Physical modeling

Figure 1 shows the schematic of the geometrical configuration under consideration. In the unperturbed condition the liquid flows along the vertical x-direction with a steady velocity and two symmetrical free interfaces. The definitions of unsteady centerline location ℓ and thickness h of the sheet are given, in terms of the interface positions $y^{\pm}$, as follows

$$\begin{aligned} \ell(x,t) &= \frac{y^{+}(x,t)+y^{-}(x,t)}{2} \\ h(x,t) &= y^{+}(x,t)-y^{-}(x,t) \end{aligned}$$

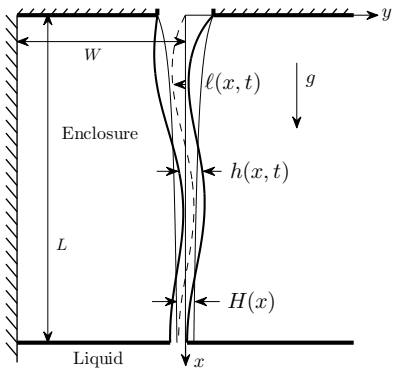

Fig. 1 Sketch of the model configuration

where superscripts $\pm$ refer to right and left interfaces, respectively, and t is the time.

We will focus our attention on the sinuous disturbances because the equations governing the evolution of the varicose modes are not able to sustain any oscillating wave pattern in the configuration here adopted, reducing to simple advection equations [4].

As rigorously derived in ([5], [6]), dimensionless equations governing the sinuous modes evolution are given by

$$\begin{cases} \dfrac{\partial \ell}{\partial t} + U\dfrac{\partial \ell}{\partial x} = v & (1) \\ \dfrac{\partial v}{\partial t} + U\dfrac{\partial v}{\partial x} = \dfrac{1}{\mathrm{We}H}\dfrac{\partial^2 \ell}{\partial x^2} - \dfrac{\mathscr{K}}{H}\bar{\ell} & (2) \end{cases}$$

while, for the steady main flow, we obtain the following non-dimensional Torricelli's free-fall solution [7]:

$$\begin{cases} UH = 1 & (3) \\ U = \sqrt{1 + 2\mathrm{Fr}\, x} & (4) \end{cases}$$

$\mathscr{K}$ is the equivalent stiffness of the air cushion, $\mathrm{We} = \frac{\rho_l U_{\mathrm{in}}^2 H_{\mathrm{in}}}{2\sigma}$ is the Weber number and $\mathrm{Fr} = gL/U_{\mathrm{in}}^2$ denotes the Froude number, being U_{in} and H_{in} the velocity and the thickness at inlet, respectively, σ the liquid surface tension and ρ_l the liquid density, L is the length curtain, $\bar{\ell}$ is the mean centerline location defined as

$$\bar{\ell} = \int_0^1 \ell \, dx.$$

The introduction of the *local* Weber number, based on the local liquid velocity $U(x)$ and local sheet thickness $H(x)$, $We_l = \frac{\rho U(x)^2 H(x)}{2\sigma}$, i.e. also, $We_l = \frac{U^2(x)}{c^2(x)}$, where $c(x) = \sqrt{\frac{2\sigma}{\rho H(x)}}$, with c being the wave velocity of sinuous disturbances (de Luca and Costa [2]), allows one to affirm that if $We > 1$, then $We_l > 1$ at each location, and the flow can be considered *supersonic*-like for the wave-patterns evolution. On the contrary, if the inlet Weber number is less than unit (i.e., *subsonic*), since the local Weber number is increasing along the downstream direction, a *transonic* location inside the sheet separates an initially *subsonic* region from a downstream *supersonic* region. Particular attention has to be paid to enforce the boundary conditions depending on whether the inlet Weber number is supersonic or subsonic. In fact, in the first case two boundary conditions are prescribed at the inlet location, $x = 0$, namely $\ell(0) = 0$ and $\frac{\partial \ell}{\partial x}(0) = 0$ (which in turn means $v(0) = 0$), whilst in the latter case the condition, $\ell(0) = 0$, has to be retained at the inlet section, and another is employed to remove the singularity of the equation and is enforced just at the singularity location [5].

3 Overall Insights

In order to give more physical insight on the fluid system under study, the equations for sinuous disturbances can be properly rearranged by taking into account integral quantities depending on the sheet extension as a whole.

Let's start to reconsider the system of equations (1-2) in terms of a single second order integro-differential equation

$$\frac{D^2\ell}{Dt^2} - \frac{U}{We}\frac{\partial^2\ell}{\partial x^2} = -\frac{\mathscr{K}}{H}\bar{\ell} \tag{5}$$

where $\frac{D}{Dt}$ is the substantial derivative. Such an equation governs the linear inviscid evolution of a generic disturbance subjected to the integral reaction term of the right hand side. The role played by the air stiffness $\mathscr{K} \geq 0$ is crucial in characterizing the dynamics of the self-sustained wave-patterns evolving into the curtain. If $\mathscr{K} = 0$ the equation is trivial, reducing to the simple wave equation with velocity $\pm\sqrt{U/We}$ relative to that of the basic flow U, basically equipped with a perfectly reflecting boundary condition at inlet, $\ell(0) = 0$, and free-outflow condition at outlet. In the fixed reference frame the wave velocity is

$$U \pm \sqrt{\frac{U}{We}} \tag{6}$$

which can also be recast in the form

$$U\left(1 \pm \sqrt{\frac{1}{We_l}}\right) \tag{7}$$

On the other hand, it is straightforward to verify that in the absence of reaction the wave equation admits solutions of the kind

$$\ell = Ae^{ik(x-at)} \tag{8}$$

where $a = U\left(1 \pm \sqrt{\frac{1}{We_l}}\right)$, k is any real wavenumber and A is a constant.

In the absence of the reaction term, one has to expect that any compact support disturbance introduced in the field splits in two parts: in supersonic conditions the one traveling on the left direction, after reflection at the inlet boundary, is eventually expelled through the right boundary as the other one, initially travelling on the right direction, does too; in subsonic local conditions both perturbations produced by the initial splitting travel towards the outlet and are expelled. Thus, if no input is introduced at the left boundary, after a finite time any solution vanishes, with the disturbance being continually expelled at the outlet of the domain. Conversely, the presence of the reaction term in the form of an integral changes things in such a way that the temporal evolution of the disturbance is by no means identically null after a finite time.

A major conjecture is that, due to the perfect reflecting character of the left boundary, at very large times the upstream characteristics is nihil potent in the sense any disturbance propagating towards the left direction will be only reflected and thus its asymptotic behavior will be the same as that the disturbances propagating on the right direction. In summary, one has to expect two-branches spectra in supersonic cases and just one branch in subsonic cases. Another relevant result is that at large times one has to expect the emergence of an unstable o less stable single mode which corresponds, as will be seen hereafter, to the response of the system behaving as a forced-damped oscillator. Of course, since the oscillator works in the driven regime, the oscillation period does not correspond to the natural frequency of oscillation and in general it cannot be determined in analytical closed form. Moreover, surface tension should have a stabilizing influence in subsonic situations (the downstream travelling modes are faster), while one can expect that the upstream directed modes of supersonic conditions are less stable. In transonic regime, when passing from subsonic to supersonic conditions, the slower branch

of the spectrum is expected to appear abruptly, whilst the faster branch should be continuous. Such predictions will be confirmed by the subsequent spectral analysis, which will be further corroborated by direct numerical simulations.

After expressing the substantial derivative in explicit form, integrating eq. (5) over the whole length of the sheet yields:

$$\bar{H}\frac{d^2\bar{\ell}}{dt^2}+2\frac{d\bar{\ell}}{dt}+\mathscr{K}\bar{\ell}=\underbrace{-2\frac{d}{dt}\int_0^1 x\frac{\partial \ell}{\partial x}dx-U\left(1-\frac{1}{WeU}\right)\cdot\left(\left.\frac{\partial \ell}{\partial x}\right|_1-\left.\frac{\partial \ell}{\partial x}\right|_0\right)}_{f_\mathrm{i}} \tag{9}$$

where f_i represents the self-induced forcing acting on the elastic oscillator. According to the development of De Rosa et al. [4], the following position has been made:

$$\bar{H}=\int_0^1 H\,dx.$$

and the boundary condition at the inlet location, $\ell(0)=0$, has been considered; quantities at the inlet and outlet boundaries are denoted with the subscripts 0 and 1, respectively. This notation will be used hereafter for all the boundary quantities. Eq. (9) exhibits a strict analogy with the motion equation of an elastic oscillator, where $\bar{H}$ denotes the mass of the liquid sheet and $\mathscr{K}$ is the equivalent spring stiffness of the enclosure air. A proper manipulation allowed one to extract a damping term. Of course, in supersonic regime it results $\left.\frac{\partial \ell}{\partial x}\right|_0=0$.

In summary, the global dynamics of the nappe consists of the mutual interaction of the centerline local deflection with the compliant air chamber which behaves as a spring acting on the average sheet deflection. Eq. (5) shows that the local deflection is forced by the global reaction term of the spring, whilst the dynamics of the global spring-mass oscillator is driven by a combination of local sheet displacement values, as described by eq. (9). In the following part of the paper we will correlate such a mutual forcing to special features of the eigenvalues spectrum; the spectrum uncovers the natural mode (possibly unstable) of the spring-mass system and the peculiar oscillating behavior of the nappe described not just by single modes, but by the superposition of a number of modes to be ascribed essentially to Eq. (5) and physically connected to another characteristic frequency linked to the typical crossing (or falling) time.

4 Linear stability analysis

A comprehensive methodology to analyze the asymptotic global behavior of the nappe dynamics consists of formulating a boundary value eigenvalues problem. This can be conveniently carried out starting from eqs. (1-2) and enforcing the global temporal modes position, i.e. by separating the variables and assuming the following form of the disturbances: $\ell(x,t)=\hat{\ell}(x)\cdot e^{\lambda t}$ and $v(x,t)=\hat{v}(x)\cdot e^{\lambda t}$, where $\hat{\ell}$ and $\hat{v}$ are the eigenfunction and λ is the complex eigenvalue. This permits one to recast the governing equations into the following compact matrical form

$$\lambda\begin{pmatrix}\hat{\ell}\\ \hat{v}\end{pmatrix}=\mathscr{A}\begin{pmatrix}\hat{\ell}\\ \hat{v}\end{pmatrix} \tag{10}$$

where the spatial operator is

$$\mathscr{A}\equiv\begin{pmatrix}-U\cdot\mathscr{D} & -\mathscr{I}\\ \frac{U}{We}\cdot\mathscr{D}^2-\dfrac{\mathscr{K}}{H}\int_0^1 dx & -U\cdot\mathscr{D}\end{pmatrix}$$

with $\mathscr{I}$ denoting the identity operator, and $\mathscr{D}$ and $\mathscr{D}^2$ the first and the second spatial derivatives, respectively.

Eigenvalues and eigenfunctions are numerically computed by means of a Chebyshev collocation method in MATLAB environment, with both differential and integral terms being spectrally accurate.

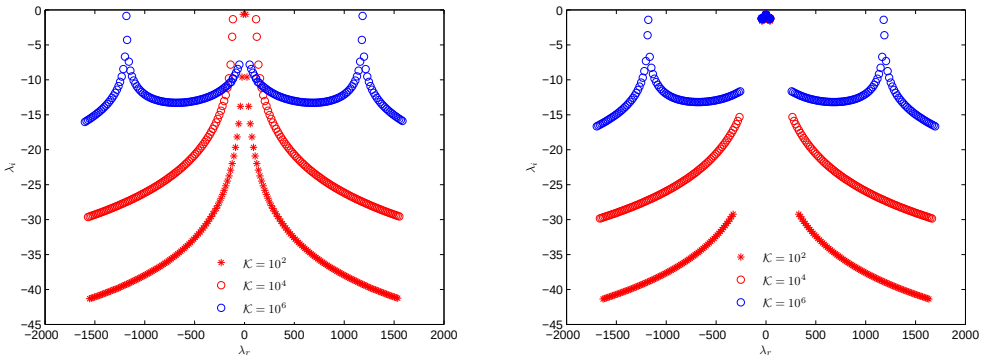

(a) (b)

Fig. 2 Spectra for $Fr = 1$ and selected $\mathscr{K}$ values. (a) $We = 0.98$, (b) $We = 1.02$.

As already anticipated before, for inlet supersonic conditions, $We > 1$, the two boundary conditions are both imposed at inlet section, i.e.

$$\hat{\ell}(0) = 0 \tag{11}$$

$$\left.\frac{\partial \hat{\ell}}{\partial x}\right|_0 = 0 \tag{12}$$

On the contrary, for inlet subsonic conditions, $We < 1$, due to the upstream directed wave characteristic velocity $U - a$, the perfectly reflecting conditions $\ell(0) = 0$ only can be retained at the inlet boundary. On the other hand for subsonic inlet at large times the eigenvalues equation becomes singular and just the condition to remove this singularity constitutes the required second boundary condition [5].

4.1 Direct numerical simulation

To corroborate the asymptotic modal analysis, direct numerical simulations of the governing equations system (1-2) have been also carried out, by means of a Crank-Nicholson finite-difference scheme, for various values of the control parameters. The initial condition is constituted by a compact support function satisfying the prescribed boundary conditions, namely a Gaussian-like pulse for the perturbed centerline of nappe, properly localized upstream or downstream of the singularity station depending on the flow regime nature, subsonic or supersonic, respectively. No perturbation in lateral velocity fluctuation v is considered here. Among the various possibilities analysed during the numerical tests, the most convenient numerical procedure appeared that based on the direct integration of the system of equations (1-2). Bearing in mind the wave nature of the expected solution, formally we imposed just the reflecting condition, $\ell(0) = 0$, on eq. (1), the free-outflow condition at the right boundary being self-guaranteed. It should be stressed that, as a consequence, at the inlet station the equation (1) is implicitly enforced as $v = U\frac{\partial \ell}{\partial x}$.

5 Results

5.1 Analysis of transonic regime

Fig. 2 compares spectra obtained in subsonic ($We = 0.98$) and supersonic ($We = 1.02$) regimes for Fr=1 and various typical values of the air stiffness $\mathscr{K}$. It should be preliminarily noted that, as expected, the subsonic regimes are characterized by one-branch only (associated to the faster travelling wave with velocity $U + \sqrt{\frac{U}{We}}$), constituted by two symmetrical parts. All the situations reported in Fig. 2(a) are stable and note that, as already extensively discussed by De Rosa et al. [4], according to the damped spring-mass model driven by the self-induced forcing f_i of eq. (9), the frequency of the less stable eigenvalue scales with $\sqrt{\mathscr{K}}$ (of course in driven

regime it coincides with that of the forcing term). Another characteristic frequency is related to the constant spacing of imaginary parts $\Delta\lambda_{\rm i}$ of eigenvalues which is related to the crossing time

$$t_{\rm cross} = \int_0^1 \frac{dx}{U \pm \sqrt{\frac{U}{We}}} \tag{13}$$

so that, by varying Froude and Weber numbers, it always results in $\Delta\lambda_{\rm i} \approx \frac{2\pi}{t_{\rm cross}}$. A further finding is the confirmation of the wave travelling feature of the solution; as will be discussed in a more quantitative detail later on, for each value of $\mathscr{K}$ here analyzed the wave velocity satisfies the relationship

$$U + a = \frac{\lambda_i}{2\pi k} \tag{14}$$

with λ_i indicating the disturbance circular frequency (i.e., the imaginary coefficient of eigenvalue) and k the wavenumber, which can be evaluated inspecting the eigenfunctions and corroborated by direct numerical simulations.

Fig. 2(b) reports three spectra for $We = 1.02$ and the same values of $\mathscr{K}$ as the previous Fig. 2(a) referring to a Weber number only slightly less than 1.02. Thus, the analysis of the two spectra yields a picture of the things when traversing the transonic region. The major feature of the present spectra is that, from one hand one notes the presence of a type of branch representing the parametric continuation of the analogous branch found for $We = 0.98$, from the other a new *nucleus* of eigenvalues having growth rate weakly less than zero clearly arises. The new nucleus of eigenvalues is to be ascribed to the travelling waves with velocity $U - \sqrt{\frac{U}{We}}$ and to their interference with another group of low frequency eigenvalues associated to the faster waves with velocity $U + \sqrt{\frac{U}{We}}$.

5.2 Details of direct numerical simulations

As asserted before, we made also systematic numerical simulations of the large time spatio-temporal evolution of the interface deflection during its transient, starting from an initial instant when a particular perturbation, typically a gaussian-like bump, was imposed to the interface shape. Generally we did not consider any initial disturbance on the lateral velocity perturbation v. The frames reported in Fig. 3 refer to the evolution computed for the subsonic case of $We = 0.82$ with $\mathscr{K} = 10^4$, and to a bump disturbance initially located at $x = 0.1$. The frames here reported show an initial bump splitting into two parts, one travelling rightwards and being rapidly expelled, the other one travelling leftwards with the expected velocities. The reflection of the left part on the inlet boundary at $x = 0$ generates the temporary establishment of a low wavenumber mode which is rapidly characterized by the appearance of shorter wavelength ripples. At large times a travelling wave, exhibiting an almost regular structure with a wavenumber of about $k = 7$, eventually establishes.

A comparison of large time sheet centerline deflections between eigenmodes (frames (a)) and direct numerical simulations (frames (b)) is reported in Figs. 4, 5, 6, corresponding to $\mathscr{K}$ equal to 100, 10^4, 10^6, respectively; the comparisons appear quite satisfactory.

5.3 Insight on supersonic regime

We would like to conclude the presentation of the results by yielding a look at the scenarios emerging in the fully supersonic regimes. A major peculiarity of the trends of the leading modes in the near supersonic field is the occurrence of characteristic high frequency ripples due to the interference of modes; such ripples structures are typically present with increasing the We number, as the leading mode evolves from a very low wavenumber to a moderate wavenumber compatible with the expected spring-mass frequency $\lambda_i = O\sqrt{\mathscr{K}}$ and fast travelling wave velocity $U + a$. The ripples disappear starting from about $We = 3.5$. Typical ripples structures are presented in plots of Fig. 7, illustrating both the leading mode shape (frame (a)) and its direct

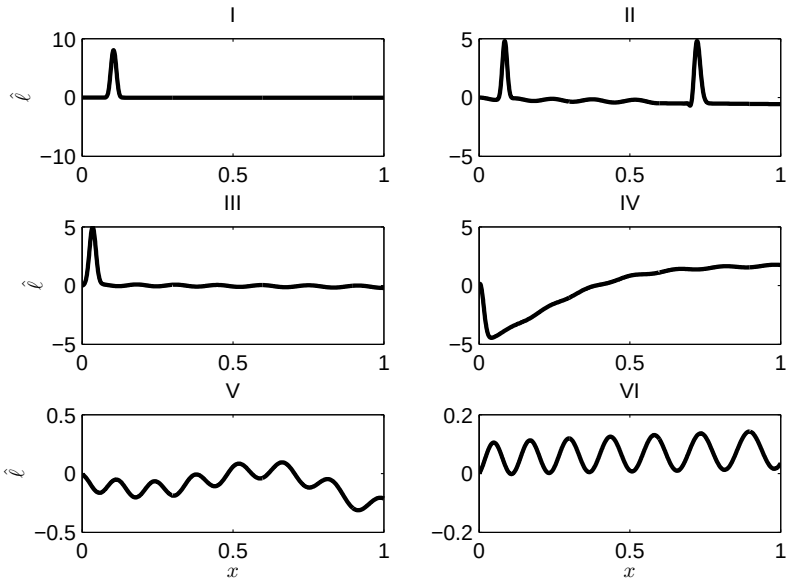

(a)

Fig. 3 Frames related to the numerical simulation for $We = 0.82$, $Fr = 1$ and $\mathscr{K} = 10^4$

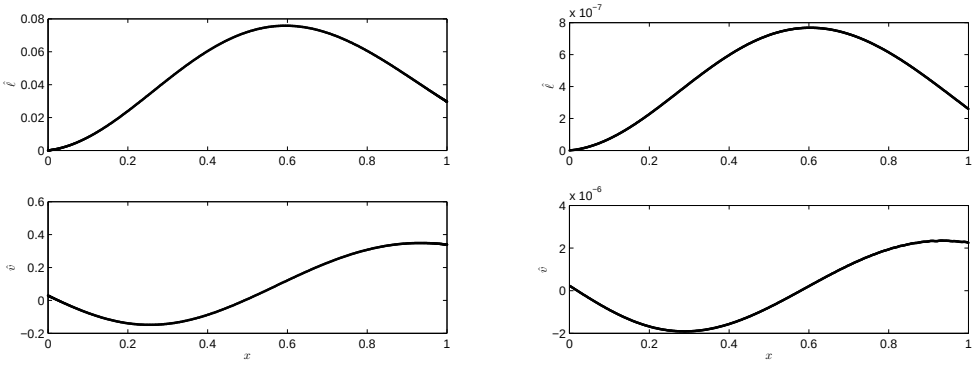

(a) (b)

Fig. 4 Comparison of eigenmode (a) and numerical simulation (b) for $We = 0.82$, $Fr = 1$ and $\mathscr{K} = 10^2$.

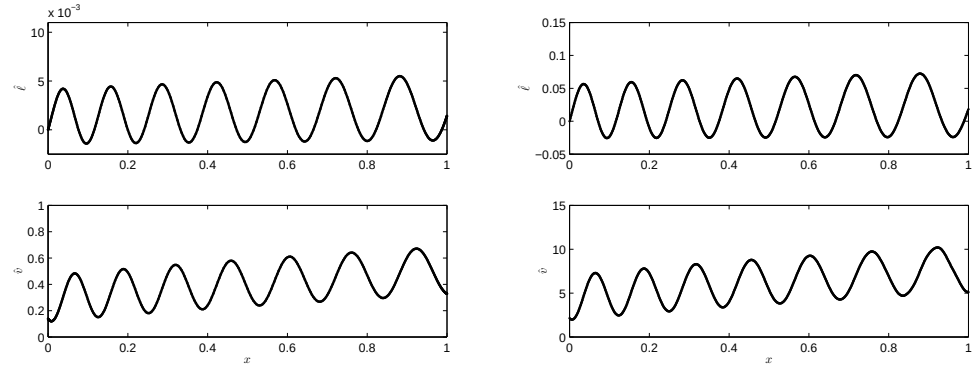

(a) (b)

Fig. 5 Comparison of eigenmode (a) and numerical simulation (b) for $We = 0.82$, $Fr = 1$ and $\mathscr{K} = 10^4$.

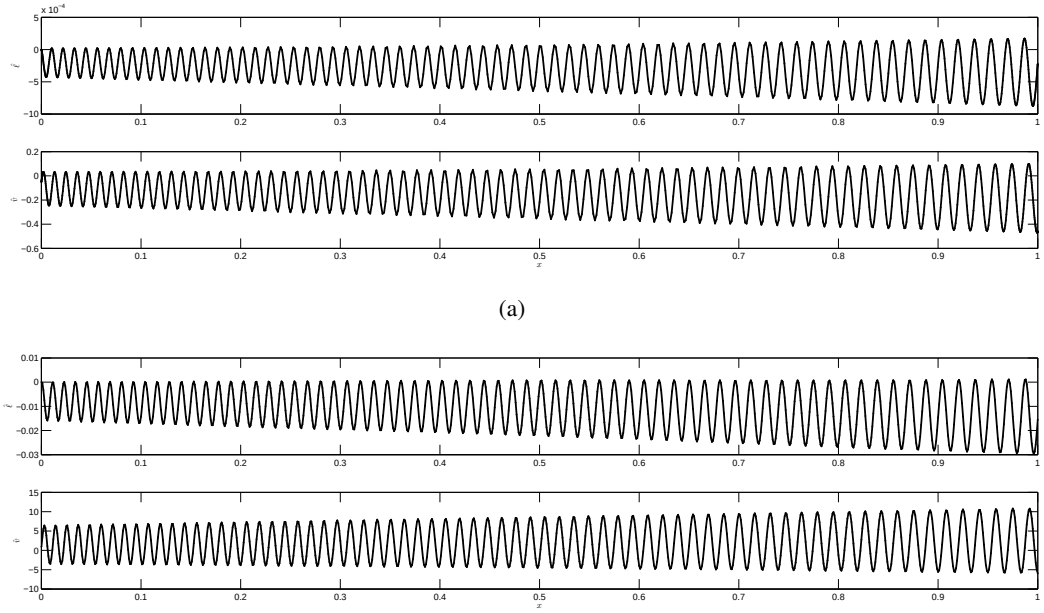

(a)

(b)

Fig. 6 Comparison of eigenmode (a) and numerical simulation (b) for $We = 0.82$, $Fr = 1$ and $\mathscr{K} = 10^6$.

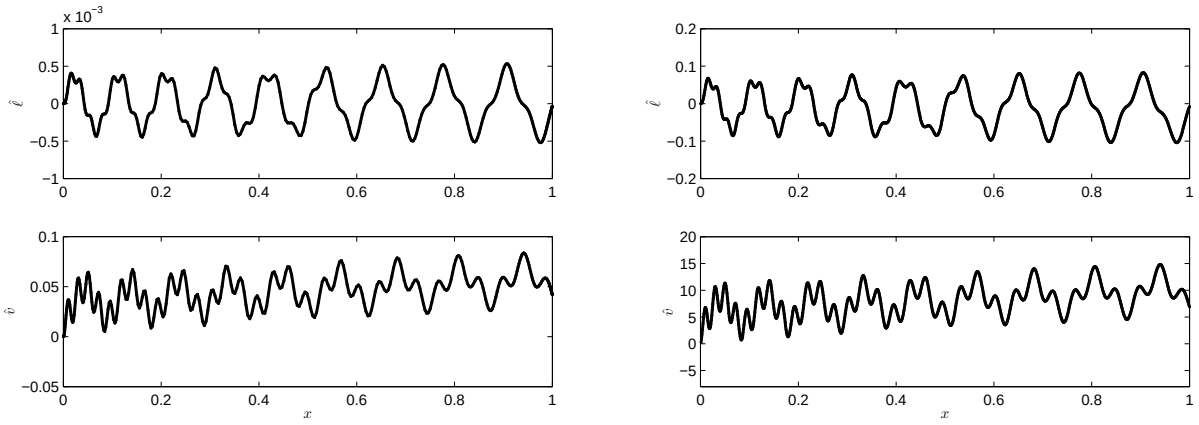

(a) (b)

Fig. 7 Leading eigenmodes (a) and direct simulations of large time behavior (b) for $We = 2.5$ and $Fr = 1$ and $\mathscr{K} = 10^4$.

simulation (frame (b)). The numerical simulations show that the ripples form due to the bits among the faster modes that go back downstream the lower modes.

It is also very interesting to compare the spectra obtained for the subsonic regime of $We = 0.98$, hence near the threshold of the transonic value, and for very high supersonic Weber numbers, tending to infinity and simulating the absence of surface tension, as illustrated in Fig. 8.

The comparison shows clearly that the leading mode frequency in the two cases here considered is practically the same, namely $\lambda_i \cong 118$. However, while the subsonic regime features an evident stability, the supersonic one without effects of surface tension is remarkably unstable, since, as deeply discussed by De Rosa et al. [4], in latter case the falling time exceeds the mass-spring period of oscillation. Since for a given frequency, the wavenumber of the leading mode is inversely proportional to the wave velocity, such a characteristic is expected in comparing the large time behaviors of nappe centerline deflection, and indeed it is visible in Fig. 9 where frame (a) refers to the subsonic case and frame (b) to the no surface tension supersonic one. Note that the supersonic wavenumber, $k \cong 13.29$, is about twice the subsonic wavenumber, $k \cong 7.18$, according to the

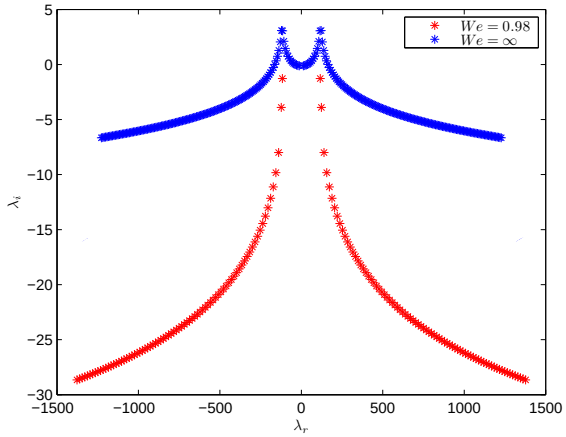

Fig. 8 Comparison of spectra for $We = 0.98$ and $We = 10^6$; in both cases, $Fr = 1$ and $\mathscr{K} = 10^4$.

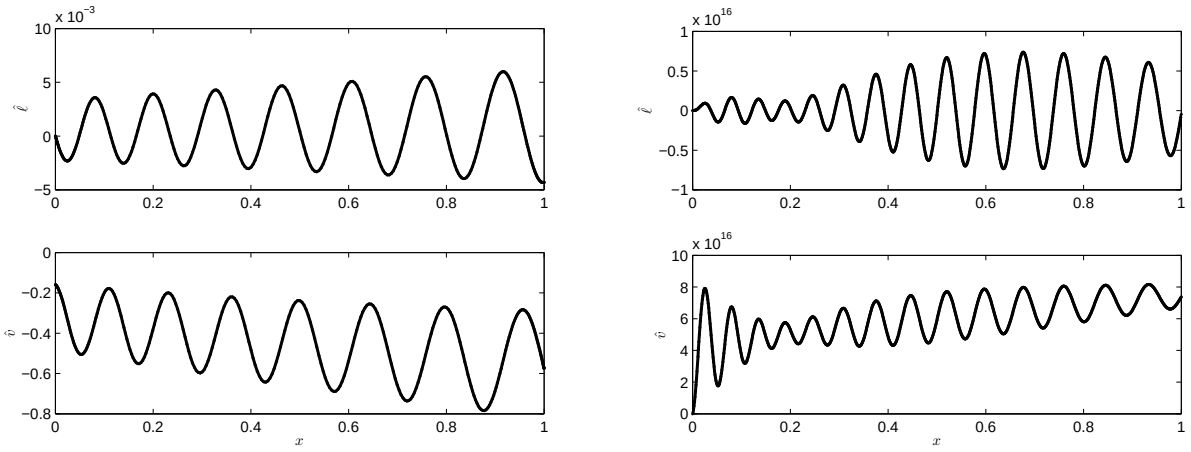

(a) (b)

Fig. 9 Direct simulations of large time behavior of leading eigenmodes for $Fr = 1$ and $\mathscr{K} = 10^4$. (a) $We = 0.96$, (b) $We = 10^6$.

circumstance that the average wave velocity is about $U = \sqrt{2}$ in the former case, and about $U = 2.62$ in the latter one.

6 Conclusion

The dynamic behavior of nappe oscillation has been revisited with reference to a physical model in which a thin liquid sheet interacts with an one-sided closed air chamber. The mutual influence of the air within the enclosure with the compliant nappe interface can produce self-induced forcing whose features have been widely investigated. The investigation has been carried out by means of both a modal (i.e., time asymptotic) linear approach, which is corroborated by direct numerical simulations of the governing equation. The unsteady dynamics has been described by means of a typical 2^{nd} order partial differential equation of hyperbolic type, showing two distinct characteristic curves. The major feature showed by a typical spectrum for We > 1 is that, from one hand one notes the presence of a type of branch representing the parametric continuation of the analogous branch found for We < 1 (associated to the faster waves) from the other a new nucleus of eigenvalues having growth rate weakly less than zero clearly arises (associated to the lower waves). The comparison of large time sheet centerline defections between eigenmodes and direct numerical simulations appears quite satisfactory. A major peculiarity of the trends of the leading modes in the near supersonic field is the occurrence of characteristic

high frequency ripples due to the interference of modes.

References

[1] Schmid P J, Henningson D S (2002) On the stability of a falling liquid curtain. *J. Fluid Mech.*, vol. 463, pp 163-171.

[2] de Luca L, Costa M (1997) Instability of a spatially developing liquid sheet. *J. Fluid Mech.*, vol. 331, pp 127-144.

[3] Weinstein S J et al. (1997) Time-dependent equations governing the shape of a twodimensional liquid curtain, part 1: Theory. *Phys. Fluids*, vol. 9, pp 3625-3636.

[4] De Rosa F, Girfoglio M, de Luca L (2014) Global dynamics analysis of nappe oscillation. *Physics of Fluids*, vol. 26, pp 122109.

[5] Girfoglio M, De Rosa F, Coppola G, de Luca L (2015) Unsteady transonic liquid sheet flows. To be submitted to *J. Fluid Mech.*

[6] Girfoglio M, De Rosa F, Coppola G, de Luca L (2013) Global eigenmodes of free-interface vertical liquid sheet flows. *WIT Trans. Eng. Sci.*, vol. 79, pp 285-295.

[7] Coppola G, De Rosa F, de Luca L (2013) Surface tension effects on the motion of a free-falling liquid sheet. *Phys. Fluids*, vol. 25, pp 062103.